Solid State Ionics 180 (2009) 1173–1182

Contents lists available at ScienceDirect

Solid State Ionics

journal homepage: www.elsevier.com/locate/ssi

Defect chemistry and oxygen transport of $(La_{0.6}Sr_{0.4-x}M_x)_{0.99}Co_{0.2}Fe_{0.8}O_{3-\delta}$, M = Ca (x = 0.05, 0.1), Ba (x = 0.1, 0.2), Sr
Part I: Defect chemistry

Bjarke Thomas Dalslet [a,b,*], Martin Søgaard [a], Henny J.M. Bouwmeester [b], Peter Vang Hendriksen [a]

[a] Fuel Cells and Solid State Chemistry Department, Risø DTU, Frederiksborgvej 399, DK-4000 Roskilde, Denmark
[b] Inorganic Membranes, MESA+ Institute for Nanotechnology, University of Twente, P.O. Box 217, 7500 AE Enschede, The Netherlands

ARTICLE INFO

Article history:
Received 28 February 2009
Received in revised form 28 April 2009
Accepted 14 May 2009

PACS:
77.84.Bw
72.60.+g

Keywords:
Mixed conductor
MIEC
Oxygen stoichiometry
Coulometric titration
LSCF
Oxide

ABSTRACT

This paper is the first part of a two part series, where the effects of varying the A-site dopant on the defect chemistry, the diffusion coefficient and the surface catalytic properties of the materials $(La_{0.6}Sr_{0.4-x}M_x)_{0.99}Co_{0.2}Fe_{0.8}O_{3-\delta}$, M = Sr, Ca (x = 0.05, 0.1), Ba (x = 0.1, 0.2) (LSMFC) have been investigated. In part I, the findings on the defect chemistry are reported, while the transport properties are reported in part II. Substitution of Sr^{2+} ions with Ca^{2+} ions (smaller ionic radius) and Ba^{2+} ions (larger ionic radius) strains the crystal structure differently for each composition while keeping the average valence of the cations constant. The Ba^{2+} containing materials show the largest oxygen loss at elevated temperatures, while the purely Sr^{2+} doped material showed the smallest oxygen loss. This was reflected in the partial oxidation entropy of the materials. The measured oxygen loss was modelled with point defect chemistry models. Measurements at very low p_{O_2} showed several phase transitions.

1. Introduction

The materials in the system $(La_{0.6}Sr_{0.4-x}M_x)_{0.99}Co_{0.2}Fe_{0.8}O_{3-\delta}$, M = Sr, Ca (x = 0.05, 0.1), Ba (x = 0.1, 0.2) (LSMFC) are mixed ionic and electronic conductors (MIECs). MIECs are interesting materials for cathodes in solid oxide fuel cells [1,2]. Other uses of MIECs exist in the field of controlled oxidation, oxygen production, or reactors for partial oxidation of methane to synthesis gas [3,4]. Current research focuses on identifying materials combining good mechanical, catalytic and oxygen permeation properties [5]. A better understanding of membrane materials can facilitate identification of materials with high thermal stability and oxygen permeability.

In perovskite materials such as LSMCF, La, Sr, Ba and Ca are usually located on the perovskite A-site, while Co and Fe reside on the B-site. La is trivalent, while Sr, Ba and Ca are divalent, and Co and Fe can have valencies of 2, 3 and 4. Due to charge balance, substitution of trivalent La for divalent Sr, Ba or Ca will be compensated by either a change in valency of Co or Fe, or by a reduction in the oxygen content of the material.

In the LSMCF materials, the amount of divalent A-site ions is kept constant. The LSMCF materials are thus not as chemically different from each other as, for instance, the series $La_{1-x}Sr_xCo_{0.2}Fe_{0.8}O_{3-\delta}$, ($x$ = 0.0, 0.2, 0.4) investigated by Tai et al. [6,7], where the valence of the A site cations is manipulated directly, or the series $La_{0.6}Sr_{0.4}Co_{1-y}Fe_yO_{3-\delta}$ (y = 0, 0.1, 0.25, 0.4, 0.6) investigated by Lankhorst and ten Elshof [8], where the B site cation is varied between the easily reducible Co and the more stable Fe ions. Substitution of Sr ions with Ca ions (smaller ionic radius) and Ba ions (larger ionic radius) will, however, perturb the crystal structure differently for each composition. The main motivation for this study is to investigate the effects of such a perturbation of the structure on the defect chemistry and the transport properties.

A number of studies have treated the effect of structure on transport properties (see e.g. Cook and Sammells [9], Stevenson et al. [10], Tsai et al. [11] or Mogensen et al. [12,13]). All these studies report on the ionic conductivity, which is a function of both the concentration of the oxide ion vacancies and the mobility of these vacancies. Furthermore some of the studies do not take the effect of oxygen exchange on the surface of the material into account. This makes it difficult to analyze why some materials are good oxygen transporters under one set of conditions, but not under another set of conditions. This paper is part I of a two-paper series that individually addresses the mobility and concentration of oxide ion vacancies as well as the

* Corresponding author. Fuel Cells and Solid State Chemistry Department, Risø DTU, Frederiksborgvej 399, DK-4000 Roskilde, Denmark.
E-mail address: bjarke.dalslet@gmail.com (B.T. Dalslet).

0167-2738/$ – see front matter © 2009 Elsevier B.V. All rights reserved.
doi:10.1016/j.ssi.2009.05.011

kinetics of oxygen exchange on the surface of the LSMCF materials. Part I reports the concentration of oxide ion vacancies. Part II reports data from measurements of the transport parameters.

The oxide ion vacancy concentration is measured using a combination of thermogravimetry (TG), and coulometric titration (CT) in a closed electrochemical cell similar to the one used by Zachau-Christiansen et al. [14]. The sample powder is placed inside a sealed zirconia cell and the oxygen content of the sample can then be controlled and measured precisely using a current supply and an amperometer. The oxygen chemical potential is measured simultaneously using a pair of reference electrodes, thus providing a precise relation between the oxygen stoichiometry in the material and the oxygen chemical potential.

To describe the defect chemistry of the materials we use two "chemical" models of different complexity. In Model I, the behavior of the overall reaction enthalpy extracted from coulometric titration is predicted by assigning different reaction enthalpies and reaction entropies to the reduction of Co^{4+} to Co^{3+} and Fe^{4+} to Fe^{3+}; In Model II, reduction of Co^{3+} to Co^{2+} is also taken into account.

2. Experimental

2.1. Sample preparation

LSMCF powders were prepared using the glycine nitrate combustion process [15]. The powders were calcined at 900 °C for 12 h, and ball milled using ZrO_2 balls, each weighing 3 g in a 500 ml polyethylene container (Ø = 5 cm) with ethanol for 24 h at 200RPM where laser inferometry showed average particle sizes below 1 μm. Shaped samples (diameter 26 mm) were pressed from this powder using uniaxial pressures of 30–70 MPa. These samples were then isostatically pressed in an evacuated latex container suspended in water at a pressure up to 325 MPa. The samples were sintered at 1300 °C for 12 h (diameter after sintering was 18.5–20 mm). The samples were polished using diamond suspensions with grain sizes down to 1 μm.

2.2. X-ray diffraction (XRD)

X-ray diffraction was done with $Cu_{k\alpha}$ radiation, with a mean wavelength of 1.5406 Å (30 mA/40 kV) on a STOE $\theta-\theta$ reflection diffractometer. The energy-dispersive, Peltier cooled Kevex detector was tuned to the $Cu_{k\alpha}$ energy (8.04 keV with an energy window of 300 eV). The step size was 0.05° and the counting time in each step was 3 s. Horizontal slits were 10 mm, and the vertical slits were 0.8 mm for the primary tube, and 0.3 mm on the detector. Sample rotation was 100 RPM. After the XRD, the sintered samples were crushed to powder for use in TG and CT.

2.3. Thermogravimetry (TG)

Powder samples were loaded into a Netzsch TG 439 differential thermobalance. An equal powder volume of alumina was used as the reference material. The powder weights were measured on a Mettler Toledo XS205 scale. Heating curves were performed in an air flow of 100 ml/min at a rate of 2 K/min: 293 K→ 1273 K→ 2 h dwell → 1273 K →293 K→1273 K → 4 h dwell. Hereafter the p_{O_2} was changed by sending, first, 100 ml/min of N_2 gas and, later, a 9%H_2/91%N_2 gas mixture through the thermobalance chamber. The p_{O_2} of the gas mixture was measured using an in-house manufactured YSZ p_{O_2} sensor downstream of the thermobalance. At 1273 K the p_{O_2} in the N_2 gas was 10^{-5} atm, and the p_{O_2} of the 9%H_2/91%N_2 mixture was 10^{-19} atm. The temperature was then increased in steps, allowing the sample to equilibrate at each step, until no further mass loss was observed. At $T = 1573$ K the sample weight changed no further.

2.4. Coulometric titration (CT)

Alumina cups with an inner diameter of 9.5 mm and a depth of 15.15 mm giving a volume of $1.07 \cdot 10^{-6}$ m^3 were used for CT. The cups were dried at a temperature, T, of 573 K and were put into an exsicator immediately after removal from the furnace. When the cups had cooled they were weighed on a Mettler Toledo XS205 scale. Each of the crushed powders were filled into a cup, and the cups with powder were dried at $T = 573$ K and put into an exsicator immediately after removal from the furnace. The weight of the powders could then be determined as the difference between the weight of the cups without powder and the weight of the cups with powder. The powder weights were all close to 2.5 g and the cup weights were all close to 7.5 g.

The setup for CT is shown in Fig. 1. $Y_{0.16}Zr_{0.84}O_{1.92}$ (YSZ) cups were machined with just enough room to contain the alumina cups. A 20 μm YSZ/$La_{0.75}Sr_{0.25}MnO_3$ (LSM) layer for pumping electrodes was spray painted on the inside and outside of the YSZ cups, and sintered at 1373 K. Hand painted porous Pt was used as current collector. Patches of porous Pt was also hand painted for reference electrodes and sintered at 1320 K. The alumina cups were inserted into the YSZ cups. Gold wires were inserted into grooves in the YSZ cups to obtain contact to the inner electrodes, through gold paint. The outer electrodes were likewise connected with attached gold wires. Two layers of in-house produced Na_2O: 17.8 mol%, Al_2O_3: 9.4 mol%, SiO_2: 72.8 mol% glass tape were attached to the bottom of the YSZ cup for sealing and the assemblies were placed on top of flat YSZ plates. Mechanical pressure was applied from the top and the bottom, and glass paste was applied at the perimeter of the YSZ cup to further strengthen the seal. The setup was slowly heated to 1273 K, with short circuited electrodes and the system equilibrated for several hours.

The majority of the measurements were performed as temperature cycles. Under open circuit conditions, to keep the oxygen content inside the compartment constant, the temperature was lowered from 1273 K to 973 K and back at a rate of 1 K/min, while the voltage between the reference electrodes was continuously recorded. After completion of a temperature cycle, and with the cell at high T, the oxygen content inside the cup was adjusted by pumping oxygen in or out, via the pumping electrodes. The amount of oxygen pumped in or out of the cup was recorded by integrating the current between the pumping electrodes. Then the temperature cycle was repeated. A Keithley 2700 multimeter was used to measure voltage and current between the electrodes. An Instek GPS3030DD power supply was used as a current source when pumping oxide ions between the pumping electrodes. The pumping current was measured as the voltage across a 10 Ω resistor. The exact resistance was measured using a Keithley 580 microΩmeter.

3. Theory

3.1. Coulometric titration (CT)

The YSZ cup is an electrochemical cell with a YSZ electrolyte. At the pumping and reference electrodes the following reaction takes place:

$$O_2(g) + 4e^- \leftrightarrows 2O^{2-}(\mathrm{YSZ}) \tag{1}$$

The Nernst equation governing the relationship between oxygen chemical potential and cell voltage is:

$$\mu_{O_2}^{in} - \mu_{O_2}^{out} = RT \ln\left(p_{O_2}^{in} / p_{O_2}^{out}\right) = 4FV_{ref} \tag{2}$$

where T is the temperature, $p_{O_2}^{in}$ and $p_{O_2}^{out}$ are the oxygen partial pressures inside and outside the cell, $\mu_{O_2}^{in}$ and $\mu_{O_2}^{out}$ are the oxygen chemical potentials inside and outside the cell, F is the Faraday constant, R is the gas constant and V_{ref} is the voltage between the reference electrodes.

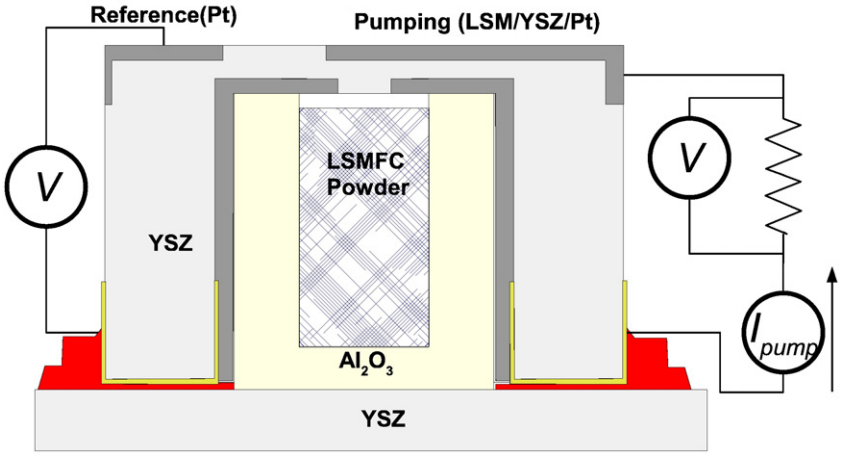

Fig. 1. Sketch of the sealed YSZ electrochemical cell used for coulometric titration. The LSMCF powder is contained in an alumina cup placed on a YSZ plate. An inverted YSZ cup with painted electrodes (dark), is lowered on top of the alumina cup. Gold paint and wires connect the electrodes to a voltmeter and a current source. The assembly is sealed with glass paste.

In this study, the gas outside the cell is atmospheric air. The standard chemical potential of oxygen as a function of T, can be calculated using the IUPAC standards for oxygen gas with the pressure $P = p_{O_2}^{out} = 0.209$ atm [16]. The chemical potential of oxygen inside the cell, $\mu_{O_2}^{in}$ can thus be found from Eq. (2):

$$\mu_{O_2}^{in} = \mu_{O_2}^{\ominus}(T,P_A) + RT\ln\left(\frac{p_{O_2}^{out}}{P_A}\right) + 4FV_{ref} \tag{3}$$

where $\mu_{O_2}^{\ominus}(T, P_A)$ is the chemical potential of oxygen at the reference pressure $P_A = 10^5$ Pa and the temperature, T. The quantity $\mu_{O_2}^{\ominus}(T,P_A) + RT\ln\left(\frac{p_{O_2}^{out}}{P_A}\right)$ can be approximated as $23442\frac{J}{mol} - 257.2\frac{J}{mol\,K}\cdot T$.

Faraday's equation gives the relationship between pumping current, I, and the oxygen transfer rate J_{O_2}. Four electrons pumped in the external circuit correspond to one oxygen molecule passing between the pumping electrodes:

$$J_{O_2} = \frac{I}{4F} \tag{4}$$

The molar amount, n, of LSMCF in the cup is $n = m/M$ where m is the mass of the powder, and M the molar mass of the perovskite. The change in δ, $\Delta\delta$, during a pumping session lasting from time t_1 to time t_2 is:

$$\Delta\delta = \frac{2M}{m}\int_{t_1}^{t_2} J_{O_2}(t)\mathrm{d}t = \frac{M}{2Fm}Q \tag{5}$$

where Q is the total charge pumped out of the cell. When the temperature is changed, or when oxygen is pumped out of the cell, the chemical potential of oxygen in the compartment is changed, and the powder will absorb or desorb the oxygen from the gas present inside the sealed cup, changing $\mu_{O_2}^{gas}$. This change can then be monitored by the reference electrodes.

For this setup, the oxygen content in the gas inside the cup corresponds to a $\Delta\delta$ of the powder inside the cup of less than 10^{-3} at $p_{O_2} = 0.215$ atm and $T = 973$ K. Furthermore, the amount of LSM in the cups was about 0.01 times the amount of LSMCF in the cup. The amount of oxygen in the gas phase, and in the electrodes inside the cup is thus much smaller than the total amount of oxygen pumped in and out of the cup and can be neglected in the data treatment.

$\mu_{O_2}^{MIEC}$ can be written down in terms of the partial molar entropy, S_{ox}, and partial molar enthalpy, H_{ox}, of oxidation.

$$\mu_{O_2}^{MIEC} = H_{ox} - TS_{ox} \tag{6}$$

H_{ox} and S_{ox} are determined by the crystal environment of the oxide ion sites, and do not directly depend on T. However, both the lattice constant [7,17] and the valency of the B-site ions are influenced by δ which *is* T-dependent. To eliminate the influence of δ, the enthalpy and entropy are calculated using T-derivatives at constant δ value.

If the powder and the gas inside the cup is in equilibrium, ($\mu_{O_2}^{MIEC} = \mu_{O_2}^{in}$), and if we assume that H_{ox} and S_{ox} are independent of T, the combination of Eq. (6) with Eq. (3) results in:

$$S_{ox} = -\left[\frac{\partial\mu_{O_2}^{MIEC}}{\partial T}\right]_\delta = -\frac{\partial\mu_{O_2}^{\Theta}}{\partial T} - R\ln\left(\frac{p_{O_2}^{out}}{P_A}\right) - 4F\left[\frac{\partial V_{ref}}{\partial T}\right]_\delta \tag{7}$$

and

$$H_{ox} = \mu_{O_2}^{\Theta} + RT\ln\left(\frac{p_{O_2}^{out}}{P_A}\right) + 4FV_{ref} + TS_{ox} \tag{8}$$

According to the data presented later in this work H_{ox} and S_{ox} are indeed independent of T, but do depend on δ.

Most of the measurements were done as temperature cycles at open circuit conditions. As the gas inside the cell only contains a very small oxygen reservoir, δ is constant during such a temperature cycle. This has the advantages, that $\left[\frac{\partial\mu_{O_2}^{MIEC}}{\partial T}\right]_\delta$ can be easily evaluated, but also that only minute amounts of oxygen need to be exchanged to obtain equilibrium between the gas and the powder, resulting in fast equilibration. The lack of hysteresis (<3 mV) between the heating and cooling curves, and the independence of the measured values on the ramp rate, confirmed that the equilibration was fast, and that the seal was intact.

3.2. Defect chemistry of LSMCF

LSMCF has a perovskite structure ABO_3, where A is a large cation and B a comparably small cation. In simple perovskites, such as $LaFeO_3$, the cations on the A (La) and B (Fe) site will have a valency of 3. Table 1 summarizes the characteristics of the ions in the LSMCF system. Ionic radii are taken from Shannon [18] and labelled with the Kröger–Vink notation with $LaFeO_3$ as reference crystal, where both La and Fe have oxidation state 3 and O has oxidation state −2.

LSMCF can be considered $MFeO_{2.5}$ (M = Sr, Ba, Ca) and $LaCoO_3$ doped $LaFeO_3$. The A-site cations are assumed to have a fixed valency. The incorporation of $MFeO_{2.5}$ in the $LaFeO_3$ lattice can, in the Kröger–Vink notation, be written:

$$2MFeO_{2.5} \overset{LaFeO_3}{\rightleftarrows} 2M'_{La} + 2Fe_{Fe}^{X} + 5O_O^X + V_O^{\bullet\bullet} \tag{9}$$

To interpret the CT data we will present different models of the defect chemistry. A common requirement is the conservation of A-site species:

$$\left[La_{La}^{X}\right] + [Sr'_{La}] + [M'_{La}] + [V'''_{La}] = 1 \tag{10}$$

Table 1
The ionic species of LSMFC.

Element	Molar mass (g/mol)	Valency	Site	Coordination number	Ionic radius (Å)
La_{La}^{X}	138.905	3	A	12	1.36
Ba_{La}'	137.327	2	A	12	1.61
Ca_{La}'	40.070	2	A	12	1.34
Sr_{La}'	87.62	2	A	12	1.44
Co_{Fe}'	58.933	2	B	6	0.745
Co_{Fe}^{X}	58.933	3	B	6	0.61
$Co_{Fe}^{\bullet}$	58.933	4	B	6	0.53
Fe_{Fe}'	55.845	2	B	6	0.78
Fe_{Fe}^{X}	55.845	3	B	6	0.645
$Fe_{Fe}^{\bullet}$	55.845	4	B	6	0.585
O_{O}^{X}	15.999	−2	O	2	1.35

Ionic radii are from Shannon [18].

We assume that the B-site is fully occupied: $[B]=[Fe]+[Co]=1$. For the transition metal species we have in the most general form, assuming that both Co and Fe may exist in di-, tri- and tetravalent form:

$$[Co_{Fe}'] + \left[Co_{Fe}^{X}\right] + [Co_{Fe}^{\bullet}] = 0.2 \tag{11}$$

and for Fe:

$$[Fe_{Fe}'] + \left[Fe_{Fe}^{X}\right] + [Fe_{Fe}^{\bullet}] = 0.8 \tag{12}$$

We assume that no interstitial sites are present in the studied materials. We also assume that the B-site ions Fe and Co are the only redox active ions.

3.2.1. Model O

In the simple model we do not distinguish between Fe and Co and will use the letter B to denote a Co or Fe ion. Furthermore, only the +3 and +4 redox states of the B ions will be taken into account. The overall reaction can be written as:

$$4B^{\bullet} + 2O_{O}^{X} \leftrightarrows O_2 + 2V_{O}^{\bullet\bullet} + 4B^{X} \tag{13}$$

The associated reaction quotient is:

$$K_{Ox} = \frac{\left[B^{X}\right]^4 [V_{O}^{\bullet\bullet}]^2 p_{O_2}}{[B^{\bullet}]^4 [O_{O}^{X}]^2} \tag{14}$$

Charge conservation states:

$$3[V_{La}'''] + [M_{La}'] = 2[V_{O}^{\bullet\bullet}] + [B^{\bullet}] \tag{15}$$

$[V_{La}'''] = 0.01$ as the LSMCF materials were synthesized with a 1% A-site substoichiometry. As the concentrations on the left side of Eq. (15) are constant, the reaction in Eq. (13) will balance the charge disparity between electron holes and oxygen vacancies.

Combining Eqs. (14) and (15) and observing that $[V_{O}^{\bullet\bullet}]=\delta$, $[O_{O}^{X}]=3-\delta$, $[B^{\bullet}]=3(1-0.99)+x-2\delta$ and $B^{X}=1-[B^{\bullet}]$ we have:

$$K_{Ox} = \frac{(1-0.03-x+2\delta)^4 \delta^2 p_{O_2}}{(0.03+x-2\delta)^4 (3-\delta)^2 P_A} \tag{16}$$

The standard Gibbs energy of the reaction in Eq. (13), ΔG_{ox} can be written:

$$\Delta G_{ox}^{\ominus} = \Delta H_{ox}^{\ominus} - T\Delta S_{ox}^{\ominus} = -RT\ln K_{Ox} \tag{17}$$

where $\Delta H_{ox}^{\ominus}$ and $\Delta S_{ox}^{\ominus}$ are the standard enthalpy and entropy of the oxidation reaction, respectively.

Combining Eqs. (2), (3), (16) and (17) we have when equilibrium is established:

$$\mu_{O_2}^{MIEC} = \mu_{O_2}^{\ominus}(T,P_A) + RT\ln\left(\frac{(0.03+x-2\delta)^4(3-\delta)^2}{(1-0.03-x+2\delta)^4\delta^2}\right) - \Delta H_{ox}^{\ominus} + T\Delta S_{ox}^{\ominus} \tag{18}$$

In terms of the partial molar entropy of oxidation we have:

$$S_{ox} = -\left[\frac{\partial \mu_{O_2}^{MIEC}}{\partial T}\right]_{\delta} = -\frac{\partial \mu_{O_2}^{\ominus}}{\partial T} \underbrace{-R\ln\left(\frac{(0.03+x-2\delta)^4(3-\delta)^2}{(1-0.03-x+2\delta)^4\delta^2}\right)}_{configurational\ entropy} - \Delta S_{ox}^{\ominus} \tag{19}$$

Mizusaki et al. [19] proposed the name configurational entropy, to the δ dependent term. In terms of the partial molar enthalpy of oxidation we have:

$$H_{Ox} = \mu_{O_2}^{\ominus}(T,P_A) - T\frac{\partial \mu_{O_2}^{\ominus}}{\partial T} - \Delta H_{ox}^{\ominus} \tag{20}$$

3.2.2. Model I

LSMCF has both Fe and Co on the B-site. The oxidation reaction in lanthanum ferrites and lanthanum cobaltites have very different enthalpies and entropies [20,21]. The different values of K_{Ox} can be taken into account by introducing the redox reaction:

$$Co_{Fe}^{X} + Fe_{Fe}^{\bullet} \leftrightarrows Co_{Fe}^{\bullet} + Fe_{Fe}^{X} \tag{21}$$

with the associated reaction quotient:

$$K_{mix} = \frac{[Co_{Fe}^{\bullet}]\left[Fe_{Fe}^{X}\right]}{[Co_{Fe}^{X}][Fe_{Fe}^{\bullet}]} \tag{22}$$

It is simple to show that:

$$K_{Ox,Co} = \frac{K_{Ox,Fe}}{K_{mix}^4} \Rightarrow \Delta H_{Ox,Co}^{\ominus} = \Delta_{Ox,Fe}^{\ominus} - 4\Delta H_{mix}^{\ominus}, \quad \Delta S_{Ox,Co}^{\ominus} = \Delta S_{Ox,Fe}^{\ominus} - 4\Delta S_{mix}^{\ominus} \tag{23}$$

where $K_{Ox,Co}$ and $K_{Ox,Fe}$ are the reaction quotients associated with the reactions found by substituting B in Eq. (14) with Co and Fe, respectively:

$$K_{Ox,Fe} = \frac{\left[Fe_{Fe}^{X}\right]^4 [V_{O}^{\bullet\bullet}]^2 p_{O_2}}{[Fe_{Fe}^{\bullet}]^4 [O_{O}^{X}]^2}, \quad K_{Ox,Co} = \frac{\left[Co_{Fe}^{X}\right]^4 [V_{O}^{\bullet\bullet}]^2 p_{O_2}}{[Co_{Fe}^{\bullet}]^4 [O_{O}^{X}]^2} \tag{24}$$

3.2.3. Model II

According to Nakamura [22] and Poulsen and Søgaard [23] who investigated $LaCoO_{3-\delta}$, Co_{Fe}' is also a possible ionic species in the perovskites. It can be taken into account by a disproportionation reaction:

$$2Co_{Fe}^{X} \rightleftarrows Co_{Fe}^{\bullet} + Co_{Fe}' \tag{25}$$

with the reaction quotient:

$$K_{dis} = \frac{[Co_{Fe}^{\bullet}][Co_{Fe}']}{[Co_{Fe}^{X}]^2} \tag{26}$$

Charge conservation now states:

$$3[V_{La}'''] + [Sr_{La}'] + [Co_{Fe}'] = 2[V_{O}^{\bullet\bullet}] + [Fe_{Fe}^{\bullet}] + [Co_{Fe}^{\bullet}] \tag{27}$$

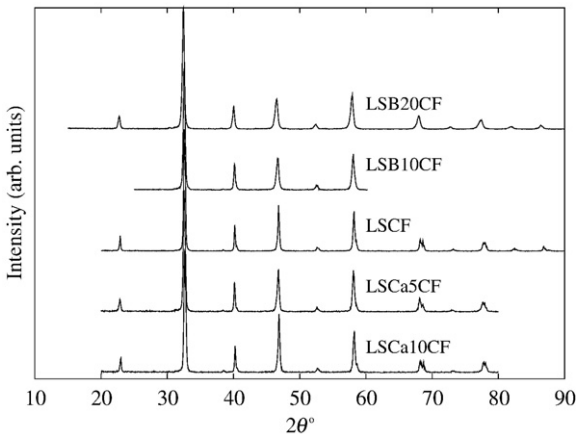

Fig. 2. X-ray diffractograms of the materials.

This model has also been discussed by Poulsen and Søgaard [23]. Solving simultaneously the Eqs. (10), (11), (12), (22), (24), (26) and (27) one may calculate all defect concentrations at a given pO2 for a given set of the parameters ($K_{Ox,Fe}$, K_{dis}, K_{mix}) of the model.

4. Results and discussion

4.1. Structure

The X-ray diffractograms recorded at $T=293$ K, of polished samples, are shown in Fig. 2, showing single phase perovskites. The detailed view of one peak in Fig. 3, shows the shift of peak position associated with different lattice constants, ρ_{XRD} are the density calculated from XRD.

In Table 2 the calculated room temperature characteristics of the powders measured by XRD are tabulated. V_F is the volume per formula unit, a and c are lattice constants.

There is a clear relation between dopant amount and V_F, with the Ba doped materials having the largest V_F and the Ca doped materials having the smallest V_F as expected considering the ionic radii of the dopants (c.f. Table 2). It is, however, unexpected that V_F of LSCF is smaller than V_F of LSCa5CF. One explanation could be that the membranes are not completely equilibrated when cooled down. As is shown later in this paper, the value of δ for LSCa5CF is larger than the value of δ for LSCF at high temperature. This difference could be "frozen in" during the cooling phase after membrane sintering, and account for this irregularity in the diffractogram.

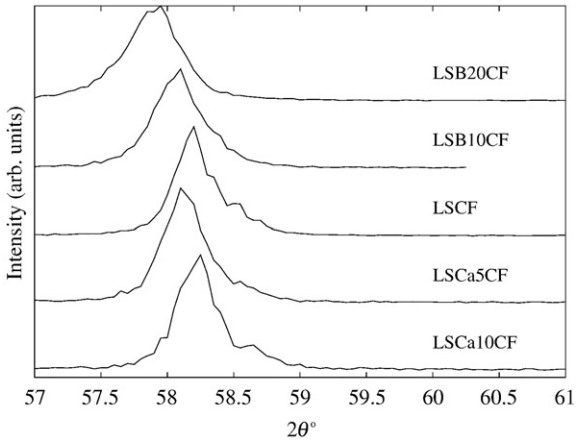

Fig. 3. X-ray diffractograms of the materials.

Table 2
Crystal structure at $T=294$ K.

Name	Dopant	x	Structure	V_F 10^{-30} m^3	a Å	c Å	ρ_{XRD} kg/m^2
LSCF	–	–	Hex.	58.3	5.50	13.38	6310
LSB10CF	Ba	0.1	Cub.	58.9	3.89	3.89	6376
LSB20CF	Ba	0.2	Cub	59.4	3.90	3.90	6481
LSCa5CF	Ca	0.05	Hex	58.7	5.59	13.47	6203
LSCa10CF	Ca	0.1	Hex	58.05	5.49	13.32	6205

4.2. Thermogravimetry (TG)

4.2.1. Total reduction

The TG measurements in air and CT measurements only give information about relative differences in δ. TG measurements, in which the powder is reduced in an N_2/H_2 mixture, were performed in order to determine the absolute value of δ. In N_2/H_2 the thermodynamically stable phases are La_2O_3, SrO, BaO, CaO, Co and Fe. The oxygen content of these phases correspond to the reduced delta $\delta_r=1.7$. The δ value of the perovskite before reduction, δ_0 can be calculated from the mass loss of reduction using:

$$\delta_0 = \delta_r - (1 - m/m_0)\frac{M}{M_0} \tag{28}$$

where m/m_0 is the normalized sample mass, m_0 being the initial mass and M_O is the molar mass of an oxygen atom.

Fig. 4 shows m/m_0 and T as a function of time, t, for an exploratory reduction attempt on LSCF. The first heating and cooling sequence until time, $t=1000$ min is done to equilibrate the powder and remove any moisture and organic residue from the system. This sequence is equivalent to the measurements shown in Fig. 5.

At $t=1192$ min the TG gas is changed to N_2 ($p_{O_2}\approx 1\cdot10^{-5}$ atm). At $t=1266$ min the gas is changed to an N_2/H_2 mixture with $p_{O_2}=10^{-19}$ atm at 1273 K, corresponding to a $p_{H_2O}\approx 4\cdot10^{-4}$ atm. This gas will approximately have $p_{O_2}=3\cdot10^{-18}$ atm at $T=1373$ K and $P_{O_2}=2\cdot10^{-16}$ atm at $T=1573$ K. In this atmosphere the sample was annealed at 1373 K until $t=2580$ min. After a cooling cycle to room temperature, the sample was taken to 1473 K, where it lost further mass. The instability during 3150 min $<t<$3880 min is attributed to pressure loss in the gas supply. Further heating to 1548 K resulted in rapid equilibration, with no further mass loss when heated to 1573 K. A surprisingly high temperature is required for complete reduction of the perovskite phase. This could be an effect of limitations in the oxygen permeability of the reduced species, that form scales around core phases which are not

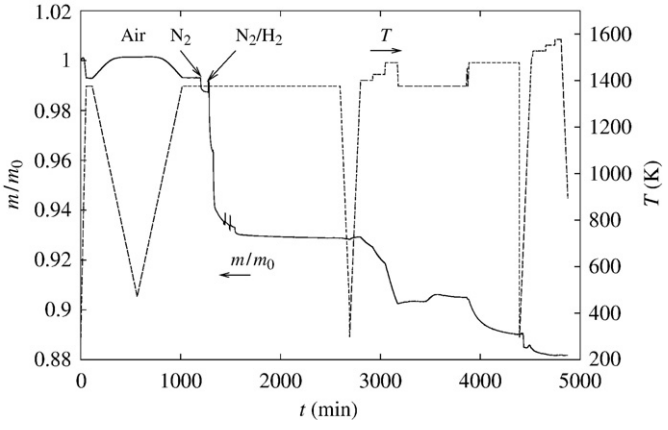

Fig. 4. T and the - normalized mass signal m/m_0 of a TG measurement of LSCF, where it was attempted to reduce the compound to the elementary oxides.

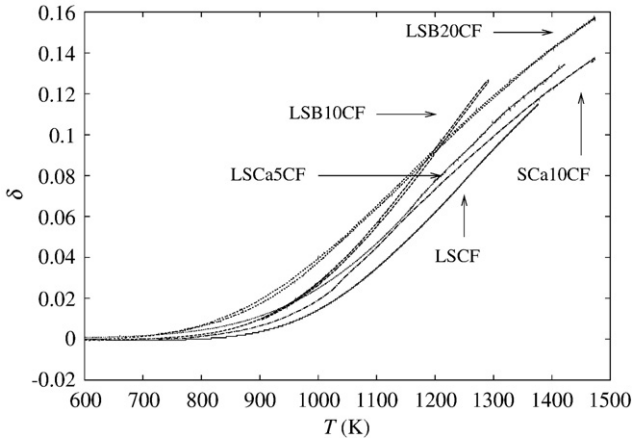

Fig. 5. δ versus T measured in air using TG.

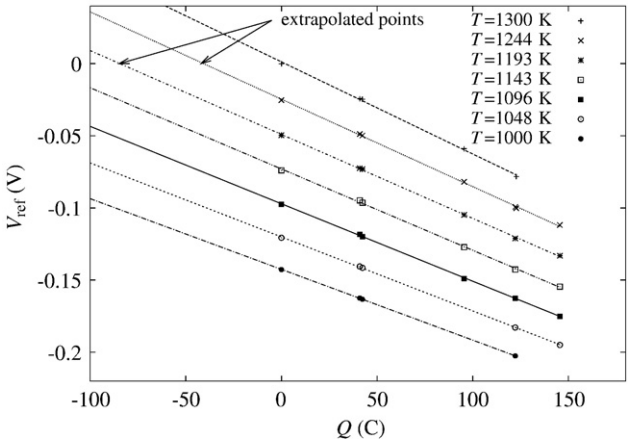

Fig. 7. The reference voltage as a function of the charge removed from the compartment, at different temperatures for the LSB10CF sample. The extrapolations are marked with arrows.

completely reduced or the formation of intermediate phases more stable than the perovskite during partial reduction.

Reduction at T up to 1573 K was repeated for all the LSMCF materials. The obtained mass loss corresponds to a room temperature δ_0 of 0 ± 0.02 for all the materials. The precision was estimated from three runs on LSB10CF resulting in calculated values of $\delta=0.003$, $\delta=0.022$ and $\delta=-0.01$ at room temperature. The low precision reflects that a change of m/m_0 of 0.01 corresponds to a δ change of 0.14. Given the uncertainty on the value of δ at room temperature, we will, in the following, assume that the room temperature δs of all the powders can be represented by the stoichiometric value of 0.

Post-measurement XRD was unsuccessful as the reduced powder quickly oxidized and hydrated in ambient atmosphere.

4.2.2. Measurements in air

In Fig. 5 δ versus T is shown for the temperature cycles in air. LSCF has the lowest mass loss, while the Ba doped samples have the highest mass loss, in agreement with the findings of Yin and Lin [24]. LSB20CF furthermore starts to lose oxygen at a lower T than the other compositions

4.3. Coulometric titration (CT)

To illustrate the data treatment we will present and discuss the results for one material, LSB10CF, in detail. Results of a coulometric titration run of LSB10CF are illustrated in Fig. 6.

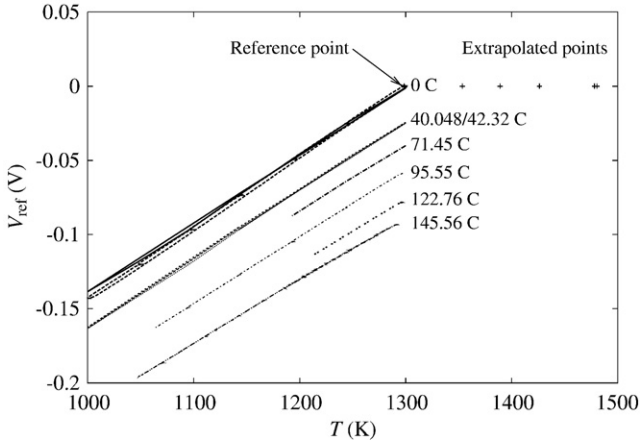

Fig. 6. V_{ref} as a function of the temperature, when different amounts of charge have been pumped from the compartment. Sample LSB10CF. Q values of 0C, 40C, 71C, 96C, 123C and 146C corresponds to $\Delta\delta$ values of 0, 0.018, 0.031, 0.042, 0.054 and 0.065.

The high degree of linearity between δ, T and $\mu_{O_2}^{MIEC}$ of LSB10CF is shared by the other LSMCF materials. A reference stoichiometry, δ_0 was selected for δ at $T=1300$ K and $\mu'_{O_2}-\mu''_{O_2}=0$ (i.e. $p^{in}_{O_2}=0.21$atm). To change δ (by $\Delta\delta$), charge was pumped out of the cell in accordance with Eq. (5).

In Fig. 6 the reference voltage as a function of the temperature, when different amounts of charge have been pumped from the compartment, is shown for LSB10CF. Each value of the charge can be converted to a δ difference, $\Delta\delta=Q/2Fn$, between the reference value, $\delta(T=1300$ K, $p_{O_2}=0.209)$ and the δ value of the powder after the pumping.

The very low hysteresis between cooling and heating runs (see Fig. 6) illustrates that drift of the signal is low and that the ionic currents can be integrated with high accuracy showing that CT is a precise method for stoichiometry determination. The relationship between log p_{O_2} (proportional to the voltage) and the temperature is perfectly linear, indicating that H_{ox} and S_{ox} are independent of temperature. This allows us to extrapolate the lines toward $V_{ref}=0$, and estimate values for the charge needed to be pumped in order to obtain equilibrium between the powder and a gas of $p_{O_2}=0.209$ atm at $T>1300$ K, providing a basis for comparison with the TG values in air.

We are able to extract H_{ox} and S_{ox} for each line in Fig. 6 using Eqs. (7) and (8).

The reference voltage as a function of the charge pumped from the compartment is shown in Fig. 7 for sample LSB10CF at different temperatures. The relationship between log p_{O_2} (proportional to the voltage) and the charge is linear. Again we extrapolate the lines toward $V_{ref}=0$, and get values for the charge needed to be pumped in order to obtain equilibrium between the powder and a gas of $p_{O_2}=0.209$ at $T<1300$ K, providing a basis for comparison with the TG values in air.

When performing the CT experiment, the glass seals were observed to be gas permeable until the cup had been annealed for some time at high temperature. This allows the powder to equilibrate with the outside atmosphere, until this sealing is complete. The absolute value of δ at the reference T, δ_0, can thus not be determined from CT and will, as mentioned, be taken from the TG measurement. Fig. 8 shows δ as a function of temperature in air obtained using TG measurements (line). The plateau at the initial warm-up phase of the TG measurement is an artifact possibly due to moist alumina powder in the reference cup; the cooldown value at $T=273$ K is used, which is considered the true $T=273$ K value of δ. The absolute values of δ from the CT measurement can be calculated from the relative values, $\Delta\delta$, as the absolute value at the chosen reference point ($T=1300$ K in air), δ_{ref} is known from the TG measurement:

$$\delta=\delta_{ref}+\Delta\delta=\delta_{ref}+Q/(2Fn) \tag{29}$$

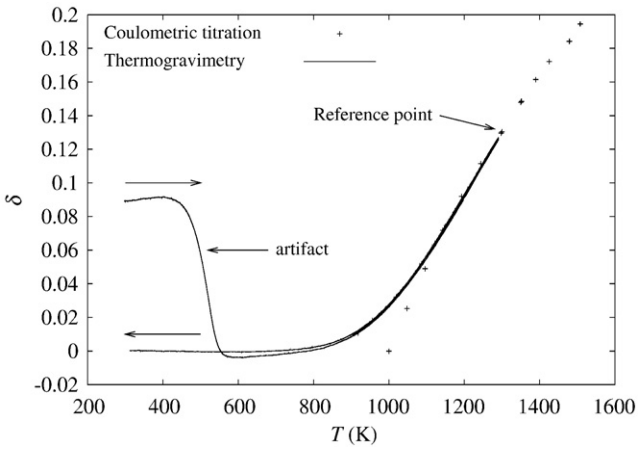

Fig. 8. Comparison of the values of δ obtained in air using TG and those extrapolated from CT experiments of sample LSB10CF. The plateau at the start of the TG measurement is an artifact possibly due to moist alumina powder in the reference cup.

The values of the CT extrapolations from Figs. 6 and 7 are compared to the TG data in Fig. 8. The errors on the extrapolated points as calculated from the standard deviations of the fits are equal to or smaller than the symbol size. There is a good agreement on the slope of both datasets around 1300 K. The extrapolated values of the CT data agree with the TG data in the range 1100 K–1300 K. The TG data and CT data deviates from each other when the extrapolations are made over large spans in T or Q (i.e. when the extrapolated point is far from 1300 K), as the assumption of linearity do not hold over these long spans.

The p_{O_2} and temperature dependence of δ at equilibrium deduced from the CT/TG measurements is plotted in Fig. 9.

The CT measurements are necessarily done in a regime where fast equilibration is possible. A contour plot of δ as a function of log p_{O_2} and T in this regime are shown for LSB10CF in Fig. 10, illustrating the area of reliable data. To get data at lower temperatures and high p_{O_2} the reference T could be set at a lower value. A reduction of T will, however, slow the pumping process considerably as the equilibration of the powder and the gas inside the cell is controlled by surface exchange processes in the powder [5,25] which are thermally activated. The equilibration will also slow down significantly at low p_{O_2} [5,25], so even at high T, pumping to very low p_{O_2} is time consuming.

If H_{ox} and S_{ox} are independent of the temperature, the contours in plots such as that in Fig. 10 will be straight lines. The straight line contours are observed in all the materials of this study.

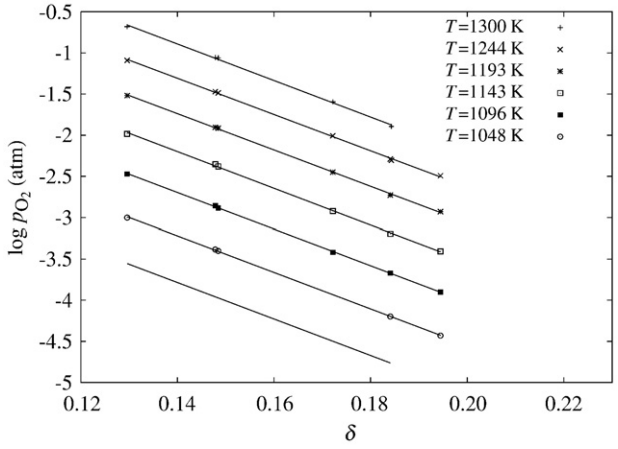

Fig. 9. log p_{O_2} as a function of δ for different temperatures for LSB10CF. Linear fits to the data are shown.

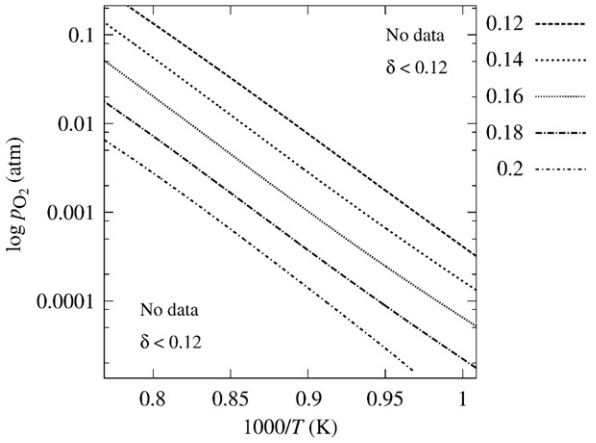

Fig. 10. Contour plot of δ as a function of log p_{O_2} and $1000/T$ for LSB10CF.

4.4. Low p_{O_2} measurement

LSCa10CF was also investigated by performing high temperature X-ray diffraction (HT-XRD) at 1198 K under various oxygen partial pressures [26]. As HT-XRD reveals the phases present in the material the p_{O_2} of the material is established via purging with gas mixtures of air, N2, or CO2/H2 and thus the precise p_{O_2} of e.g. a phase transition can be impossible to obtain. In CT, however, the pumped charge directly controls δ and thus provides equilibrated measurements of the p_{O_2} even at phase transitions.

A well-sealed CT cell is capable of reaching very low p_{O_2} through long pumping runs. At $p_{O_2} < 10^{-4}$ atm in an oxygen/nitrogen mixture, the surface exchange for these materials becomes too slow to pump and measure $\mu_{O_2}^{MIEC}$ at the same time [5], and only discrete measurement points after equilibration can be recorded.

δ is plotted as a function of p_{O_2} for LSCa10CF in Fig. 11. The curve is measured while pumping continuously, while the discrete point values are taken after powder equilibration. The points are taken during several pump cycles, and we observe that the behavior is reversible and reproducible.

According to the results of Søgaard et al. [20,21] at $p_{O_2} > 10^{-6}$ atm the B-site cations of $(La_{0.6}Sr_{0.4})_{0.99}CoO_{3-\delta}$ and $(La_{0.6}Sr_{0.4})_{0.99}FeO_{3-\delta}$ can have valences of both 4+ and 3+. In the case of Co ions the valency can even be below 3. This gives a smooth δ dependence on μ_{O_2} as no phase transitions are involved. HT-XRD [26] revealed that for p_{O_2}-values between 0.2 atm and $\approx 10^{-4.5}$ atm the material is a single phase

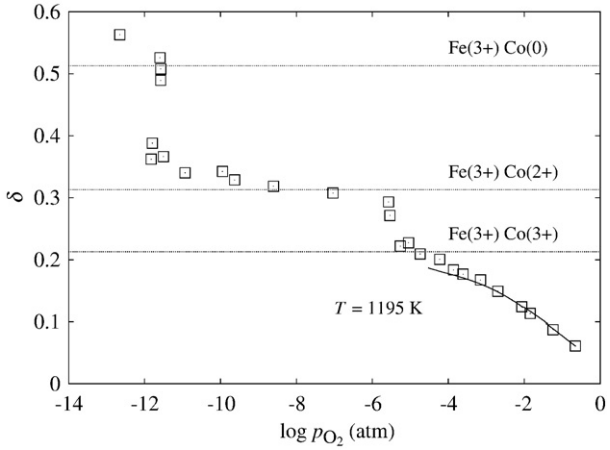

Fig. 11. δ as a function of p_{O_2} for LSCa10CF. At high p_{O_2} a continuous curve can be recorded while pumping, while measurements at low p_{O_2} require equilibration of the powder and gas inside the cell resulting in point values.

perovskite. Thus we attribute the curve at $p_{O_2} > 10^{-6}$ atm to the redox reactions between Co'_{Fe}, Co^x and $Co^{\bullet}_{Fe}$; and between Fe^x and $Fe^{\bullet}_{Fe}$.

A HT-XRD diffractogram recorded at $p_{O_2} \approx 10^{-10}$ atm, showed the same perovskite peaks as the diffractogram recorded at $p_{O_2} \approx 10^{-4.5}$ and additional peaks ascribable to $Co_{1-x}Fe_xO$ together with two new peaks of a non-identified phase. In the CT measurement we see that at $0.21 < \delta < 0.3$ at $\log p_{O_2} = 10^{-6}$ atm, a phase transition takes place. Only a slight change in the chemical potential of oxygen inside the cell was measured, even when the apparent δ was changed substantially. If all the Fe and Co cations are in the +3 valence state, δ is 0.213 (if the ratio of A site and B site cations was 1:1, δ would be 0.2, however, the ratio of the A and B site cation have been synthesized to 0.99:1 and according to charge neutrality we obtain $\delta = 0.213$). Having all the Fe in the +3 state and all the Co in the +2 state corresponds to $\delta = 0.313$. The step in δ from $\approx 0.21 \rightarrow \approx 0.31$ is thus attributed to the reduction of Co^X, and partial decomposition of the perovskite as found in HT-XRD. Nakamura et al. [22] found a similar behavior for $LaCoO_3$.

For $\delta > 0.21$ where the perovskite partially decomposes, the meaning of the measured δ changes; instead of referring to the oxygen substoichiometry of a single well known perovskite in the cup, it now refers to the total difference in oxygen content between all the powders in the cup and the stoichiometric reference perovskite originally present in the cup.

At $0.31 < \delta < 0.32$ ($10^{-5.5}$ atm $< \delta < 10^{-12}$ atm) there is a large change in $\mu^{MIEC}_{O_2}$ with little change in δ. No changes were detected in HT-XRD spectra in this p_{O_2} interval [26]. We attribute this to the reluctance of both Co^{2+} [22] and Fe^{3+} [21] to be reduced any further for $p_{O_2} > 10^{-11.5}$ atm.

HT-XRD [26] revealed that at $p_{O_2} \approx 10^{-14.5}$ atm signs of peaks ascribable to metallic Co (possibly with some Fe dissolved) are observed. At $p_{O_2} \approx 10^{-15.7}$ these becomes clearly identifiable as well as peaks ascribable to (La,Sr,Ca)(Fe,Co)O_4. If all the Fe is Fe^{3+} and all the Co is metallic cobalt (Co^0), δ will be 0.513. At $p_{O_2} \approx 10^{-12}$ atm CT shows a step between $0.32 < \delta < 0.52$ that is thus interpreted as the complete reduction of Co^{+2} to metallic Co(s). The discrepancy between the p_{O_2} values of this phase transition between XRD and CT is ascribed to possible errors on the temperature determination in the experiments and also that equilibrium is not fully established in the X-ray experiments. This is consistent with the measurements of Nakamura et al. [22] on $LaCoO_3$.

4.5. p_{O_2} dependence of δ for all materials

Comparisons of the p_{O_2} dependence of δ at $T = 973$ K and $T = 1173$ K for different materials are shown in Figs. 12 and 13,

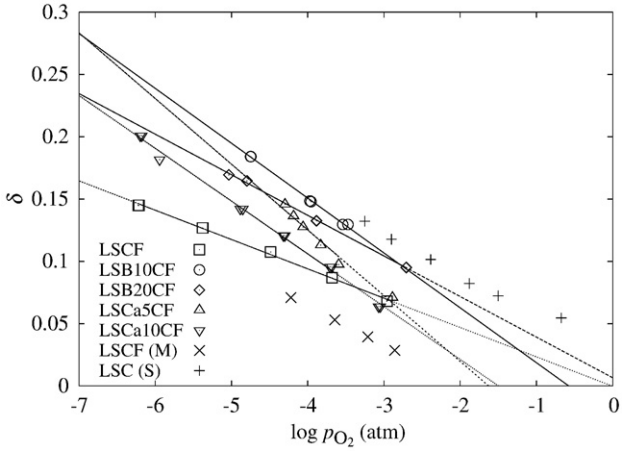

Fig. 12. Comparison of the p_{O_2} dependence of δ for different materials. $T = 973$ K. LSCF (M) and LSC are values for LSCF and $(La_{0.6}Sr_{0.4})_{0.99}CoO_{3-\delta}$ obtained by Mantzavinos [27] and Søgaard [20], respectively.

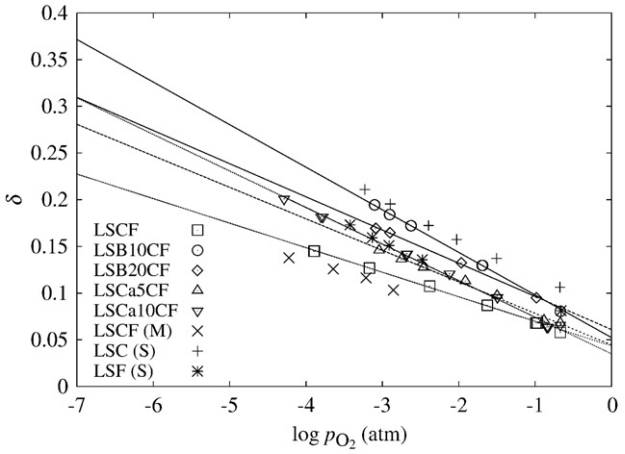

Fig. 13. Comparison of the p_{O_2} dependence of δ for different materials. $T = 1173$ K. LSCF (M), LSC and LSF are values for LSCF, $(La_{0.6}Sr_{0.4})_{0.99}CoO_{3-\delta}$ and $(La_{0.6}Sr_{0.4})_{0.99}FeO_{3-\delta}$ obtained by Mantzavinos [27], Søgaard [20] and Søgaard [21], respectively.

respectively. We have compared the LSMCF results to those of LSCF reported by Mantzavinos [27] in a similar experiment. Good agreement for LSCF is found at 1173 K.

Ba on the A-site in the LSMCF materials leads to a comparably high vacancy concentration. When the A-site contains Ca, the vacancy concentration is lower than when the A-site contains Ba but still higher than in LSCF, which is the most redox stable of the LSMCF compounds.

The vacancy concentrations of $(La_{0.6}Sr_{0.4})_{0.99}CoO_{3-\delta}$ reported by Søgaard et al. [20] are slightly higher than those of LSB10CF. The vacancy concentrations of $(La_{0.6}Sr_{0.4})_{0.99}FeO_{3-\delta}$ $T = 1173$ K reported by Søgaard et al. [21] is similar to those we find for LSCa10CF. It is remarkable that, according to the values reported by Søgaard et al., the difference between LSCF and LSB10CF is, in this p_{O_2} and temperature range, larger than the difference between $(La_{0.6}Sr_{0.4})_{0.99}CoO_{3-\delta}$ and $(La_{0.6}Sr_{0.4})_{0.99}FeO_{3-\delta}$. A change of 10% of the A-site cations from the small Sr^{2+} ion to the large Ba^{2+} ion is as important, in terms of the ease with which vacancies are generated, to a change of all the B site cations from Fe to the easier reducible Co. The crystal structure (or the nature of the alkaline earth element) thus has a strong impact on the defect chemistry.

4.6. H_{ox} and S_{ox}

H_{ox} was extracted from the coulometric titration data. The extracted values are shown as a function of δ in Fig. 14.

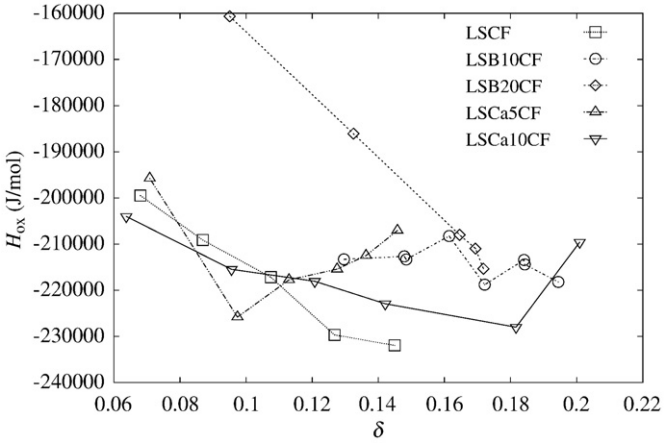

Fig. 14. H_{ox} as a function of δ. The connecting lines are guides to the eye. The confidence interval widths are much smaller than the symbol size.

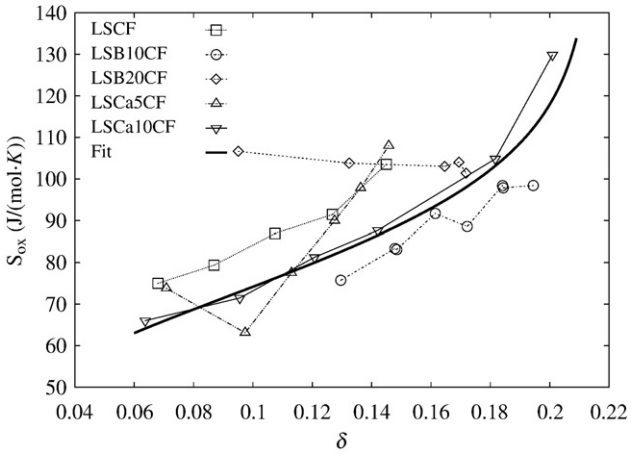

Fig. 15. S_{ox} as a function of δ for the different materials. A fit to Eq. (19) for LSCa10CF has been added. The connecting lines are guides to the eye. The confidence interval widths are comparable to the symbol size or less.

With the exception of LSB20CF and LSCF, the variation of H_{ox} as a function of δ is weak, suggesting a single B-site cation reaction being responsible for the reaction. In the case of LSB20CF and LSCF, the variation suggests that several reactions are simultaneously responsible.

S_{ox} was extracted from the coulometric titration data. The extracted values are shown as a function of δ in Fig. 15. A trendline based on Eq. (19) can be vertically adjusted to fit the measurement series confirming that the delta dependence of S_{ox} can be well described by Eq. (19). An exception is LSB20CF, that has a δ independent S_{ox}. The δ dependence of H_{ox} of LSB20CF is also much stronger than for the other materials. Hence, the reduction mechanism in this sample seems different from the others.

For the LSMCF materials (excluding LSB20CF), the most easily reducible materials (see Figs. 12 and 13) are the ones with the lowest values of S_{ox} at any given value of δ. No direct coupling between reducibility and H_{ox} is seen.

As H_{ox} and S_{ox} are independent of temperature (see Fig. 10), the data in Figs. 14 and 15 contains all the information of the coulometric titration measurements (except for the low p_{O_2} measurements of Fig. 11). Inserting H_{ox} and S_{ox} for a given δ into Eq. (6) and combining with Eq. (3) will reproduce these measurements in their entirety.

4.7. Model fits

The oxygen nonstoichiometry data for all the materials was fitted to the models described in Section 2. An example for LSB10CF, with

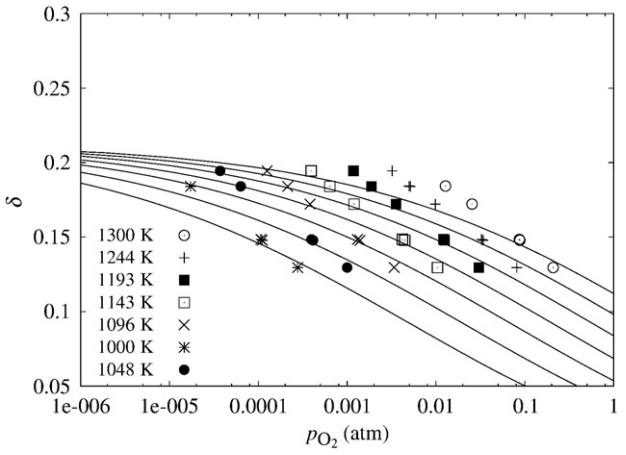

Fig. 16. Fit of data measured on LSB10CF to Model I. Only data for which δ<0.15 have been used in the fit.

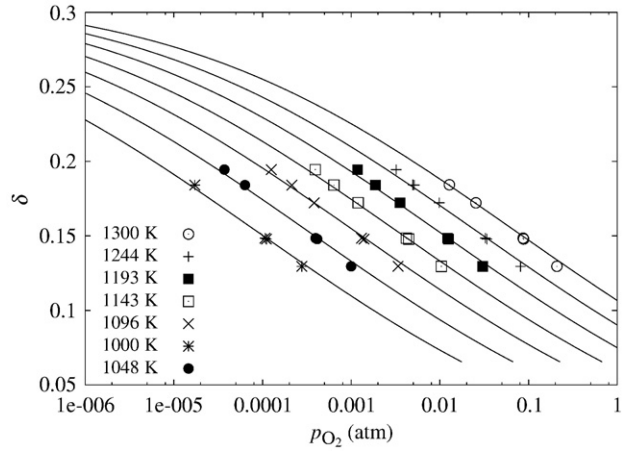

Fig. 17. Fit of data measured on LSB10CF to Model II.

Model I and Model II is shown in Figs. 16 and 17, respectively. Model I is not able to reproduce the data at δ>0.15, as it does not take the reduction into the +2 valence state of the B ions into account. Model I is thus only able to fully reproduce the measurements of LSCF and LSCa5CF, for which δ<0.15 under all the conditions of measurement. Model II is able to replicate the data precisely for all the materials.

4.8. Parameter extraction

The fitting parameters providing the best fit to the measurements, and their confidence intervals, shown below each fitting value, are compared to the measured values of H_{ox} and S_{ox} in Table 3 for Model I.

The measured parameters, tabulated in Table 3 are the values for $\delta = 0.12$ (See Figs. 14 and 15), while the interval tabulated below each value is the spread of these values in the measurements of this study. ln K_{ox} is calculated at $T = 1173$ K for $\delta = 0.12$.

Model I was used on all the materials, but only for measurement points with δ<0.15, as it could not model the data satisfactorily for higher δ values. This, unfortunately, means that the measurements on LSB10CF and LSB20CF are only fitted in a few points, and the precision of the fits of those materials suffers accordingly. On the other hand, one set of $H_{ox,Co}$, $S_{ox,Co}$, $H_{ox,Fe}$, $S_{ox,Fe}$ values could be used to fit all δ values below 0.15. From this set $K_{ox,Co}$ and $K_{ox,Fe}$ was calculated for $T = 1123$ K. The interval tabulated below each value represents the 68% confidence interval based on those fits.

According to Eq. (23), K_{ox} should be a convolution of the Co- and Fe-specific reaction constants of Model I, $K_{ox,Co}$ and $K_{ox,Fe}$. The fitted values for LSCF, LSCa5CF and LSCa10CF agree with this inside their wide confidence intervals. These measurements can, however, not easily distinguish between a change of valence state of Co or Fe; this is

Table 3
Fitting parameters of best fit for three of the compositions.

	Measured			Model I	
	H_{ox}	S_{ox}	lnK_{ox}	ln$K_{ox,Co}$	ln$K_{ox,Fe}$
	kJ/mol	J/(mol K)	–	–	–
LSB20CF	−178	105	−4.4	4	−15
	−215 ↔ −159	102 ↔ 108	–	−5 ↔ 4	−22 ↔ −12
LSB10CF	−210	78	−4.5	24	−9
	−218 ↔ −209	78 ↔ 100	–	0 ↔ 24	−35 ↔ −9
LSCF	−226	90	−7.5	47	24
	−232 ↔ −198	76 ↔ 103	–	20 ↔ 48	20 ↔ 25
LSCa5CF	−216	84	−5.8	66	13
	−225 ↔ −207	58 ↔ 108	–	20 ↔ 96	−23 ↔ 19
LSCa10CF	−218	82	−5.8	41	4
	−228 ↔ −204	65 ↔ 130	–	0 ↔ 58	−62 ↔ 13

Below each parameter fit value is shown the parameter value intervals of points resulting in a χ^2 value less than 2.

reflected in the wide confidence intervals, where a too large value for Fe is compensated by a too low value for Co. We can thus not, from these fits alone, extract much knowledge of the balance between oxidation of Co and Fe.

Model II, which has six fitting parameters, has even wider confidence intervals than Model I. It is, however, capable of very high quality fits of the data for all δ values. Lankhorst and ten Elshof made measurements on LSCF with different ratios of Co to Fe on the B-site. This enabled them to estimate fitting parameters dependent of the Co/Fe ratio, and reduce the number of fitting parameters while maintaining high precision in the replication of their measured data. The model of Lankhorst and ten Elshof could replicate our results, however, the value of the parameters fixed by Lankhorst and ten Elshof were not valid for our measurements. These parameters needed to be fitted independently, and the resulting confidence intervals were as large as those of Model II.

In conclusion it was not possible to model the results with a few well determined fitting parameters applicable to all values of δ. Increasing the model complexity, and the number of fitting parameters, gave excellent reproduction of the measured data, but widened the confidence intervals.

5. Conclusions

In this study, the system, $(La_{0.6}Sr_{0.4-x}M_x)_{0.99}\ Co_{0.2}Fe_{0.8}O_{3-\delta}$, M = Ca, Ba, Sr, was investigated using X-ray diffraction (XRD), thermogravimetry (TG) and coulometric titration (CT). TG reduction in a N_2/H_2 gas mixture at $T>1498$ K revealed the absolute oxygen substoichiometry, δ, which was found to be close to 0 at room temperature for all the materials. TG and CT allowed the relation between δ and the oxygen activity at $T>873$ K to be measured with high precision. The results of TG and CT were in good agreement. Substitution of Sr with Ca and Ba increased the reducibility the investigated materials. Enthalpies and entropies of oxidation could be extracted for each material. Due to the high number of ionic species in these materials, it was impossible to extract detailed knowledge of the redox reactions in the material, from the applied defect chemistry models.

Acknowledgement

The authors would like to acknowledge Christodoulos Chatzicheristodoulou for providing HT-XRD data.

References

[1] P. Gellings, H. Bouwmeester, The CRC Handbook of Solid State Electrochemistry, CRC Press, 1997.
[2] S.J. Skinner, J.A. Kilner, Mater. Today 6 (2003) 30.
[3] P.V. Hendriksen, P.H. Larsen, M. Mogensen, F.W. Poulsen, K. Wiik, Catal. Today 56 (2000) 283.
[4] H.J.M. Bouwmeester, Catal. Today 82 (2003) 141.
[5] B. Dalslet, M. Søgaard, P.V. Hendriksen, J. Electrochem. Soc. 154 (2007) (12).
[6] L.-W. Tai, M. Nasrallah, H.U. Anderson, J. Solid State Chem. 118 (1995) 117.
[7] L.W. Tai, M. Nasrallah, H.U. Anderson, D. Sparlin, S. Sehlin, Solid State Ion. 76 (1995) 273.
[8] M.H.R. Lankhorst, J.E. ten Elshof, J. Solid State Chem. 130 (1997) 302.
[9] R.L. Cook, A.F. Sammels, Solid State Ion. 45 (1991) 311.
[10] J. Stevenson, T. Armstrong, R. Carnheim, L. Pederson, W. Weber, J. Electrochem. Soc. 143 (1996) 2722.
[11] C. Tsai, A. Dixon, Y. Ma, W. Moser, M. Pascucci, J. Electrochem. Soc. 81 (1998) 1437.
[12] M. Mogensen, D. Lybye, N. Bonanos, P.V. Hendriksen, Adv. Sci. Technol. 29 (2000) 1261.
[13] M. Mogensen, D. Lybye, N. Bonanos, P. Hendriksen, F. Poulsen, Solid State Ion. 174 (2004) 279.
[14] B. Zachau-Christiansen, T. Jacobsen, S. Skaarup, Solid State Ion. 86–88 (1996) 725.
[15] L.A. Chick, G.L. Maupin, L.R. Pederson, D.E. McCready, J.L. Bates, Mater. Res. Soc. Symp. Proc. 249 (1992) 159.
[16] W. Wagner, K.M. de Reuck, IUPAC International Tables of the Fluid State vol. 9, 1988.
[17] W. Wang, R. Barfod, P. Larsen, K. Kammer, J. Bentzen, P. Hendriksen, M. Mogensen, Improvement of LSM cathode for high power density SOFC, SOFC VIII (Paris) proceedings, 2003, p. 400.
[18] R.D. Shannon, Acta Crystallogr. A32 (1976) 751.
[19] J. Mizusaki, S. Yamauchi, K. Fueki, A. Ishikawa, Solid State Ion. 12 (1984) 119.
[20] M. Søgaard, P.V. Hendriksen, M. Mogensen, F.W. Poulsen, E. Skou, Solid State Ion. 177 (2006) 3285.
[21] M. Søgaard, P.V. Hendriksen, M. Mogensen, Oxygen nonstoichiometry and transport properties of strontium substituted lanthanum ferrite, J. Solid State Chem. 180 (2007) 1489.
[22] T. Nakamura, G. Petzow, L.J. Gauckler, Mater. Res. Bull. 14 (1979) 649.
[23] F.W. Poulsen, M. Søgaard, Proceedings of The fifth European Solid Oxide Fuel Cell Forum, vol. 2, 2002, p. 687.
[24] Q. Yin, Y.S. Lin, Adsorption 12 (5–6) (2006) 329.
[25] J. ten Elshof, M. Lankhorst, H. Bouwmeester, Chemical diffusion and oxygen exchange of $La_{0.6}Sr_{0.4}Co_{0.2}Fe_{0.8}O_{3-\delta}$, Solid State Ionics 99 (1997) 15.
[26] C. Chatzicheristodoulou, Unpublished results.
[27] D. Mantzavinos, A. Hartley, I.S. Metcalfe, M. Sahibzada, Oxygen stoichiometries in $La_{1-x}Sr_xCo_{1-y}Fe_yO_{3-\delta}$ perovskites at reduced oxygen partial pressures, Solid State Ionics 134 (2000) 103.